Available online at www.sciencedirect.com
SCIENCE DIRECT
International Journal of Heat and Fluid Flow 26 (2005) 843–854
International Journal of HEAT AND FLUID FLOW
www.elsevier.com/locate/ijhff

On trailing vortices: A short review

Laurent Jacquin *

ONERA/Department of Fundamental–Experimental Aerodynamics, 8 rue des Vertugadins, 92190 Meudon, France

Abstract

This paper reviews some mechanisms involved in the dynamics of vortices in fluid flows. The topic is first introduced by pointing out its importance in aerodynamics. Several basic notions useful to appraise experimental observations are then surveyed, namely: centrifugal instabilities, inertial waves, cooperative instabilities, vortex merger, vortex breakdown and turbulence in vortices. Each topic is illustrated with experimental or numerical results.

Keywords: Vortices; Hydrodynamic instability; Turbulence; Aerodynamics

1. Introduction

A lifting wing is conceived so as to deflect part of the impinging flow momentum into a normal component. This produces, by reaction, a normal force which is opposite to this momentum component. As shown by the wind tunnel experiment of Fig. 1, in the case of a finite wing, this produces trailing vortices. After the merger of different vortices produced by the wing elements, a single pair of counter-rotating vortices forms. The flux of momentum of this vortex system is equal and opposite to the lift of the vortex generator (here a complete aircraft). The same mechanism holds in a jet deflected by a cross-flow, in which a vortex pair also forms and conveys the vertical momentum of the jet. In the two above cases, the trailing vortices are associated to a momentum deflection which is due to the work of the viscous and turbulent stresses taking place in the wing boundary layer, in the case of the wing, or in the jet mixing layer, in the case of a jet normal to a cross-flow (shocks also contribute in supersonic regimes). The corresponding energy is momentarily stored in a trailing vortex system and could, in principle, be restored before completion of the wake dissipation. In the case of an aircraft, this energy is equal to the work of the "induced drag" or "vortex drag", which amounts to a third of the total drag, typically. This means that a third of the power delivered by the propulsion unit of an aircraft is used for the lift and is momentarily stored in vortices. Once vortices are formed, they last on a long distance and they may produce undesirable loads on structures or upset rolling momentum on following vehicles. Aerodynamic applications, such as aircraft wake hazard alleviation (see Crouch and Jacquin, 2005) or vortex breakdown control, have stimulated researches on the prediction and/or the control of these vortices. This paper gives an overview of these findings. Its main objective is to draw attention on some fundamental results which may be useful to analyse flows dominated by vortices. The review begins with considerations on the stabilizing/destabilizing effects of rotation and/or curvature (see Section 2). Section 3 is devoted to the stability properties of a vortex. In this section we detail the mechanisms responsible for the persistence of trailing vortices and we explain how this intrinsic stability may be mitigated. A short discussion on vortex breakdown follows (see Section 4). Section 5 is devoted to the stability of vortex systems and Section 6, to buoyancy effects in vortices. Every notion is exemplified with experimental and/or numerical results. Problems common to the experimental characterizations of trailing vortices are briefly discussed in the last section.

* Tel.: +33 1 46 23 51 53; fax: +33 1 46 23 51 58.
E-mail address: jacquin@onera.fr

0142-727X/$ - see front matter © 2005 Elsevier Inc. All rights reserved.
doi:10.1016/j.ijheatfluidflow.2005.10.001

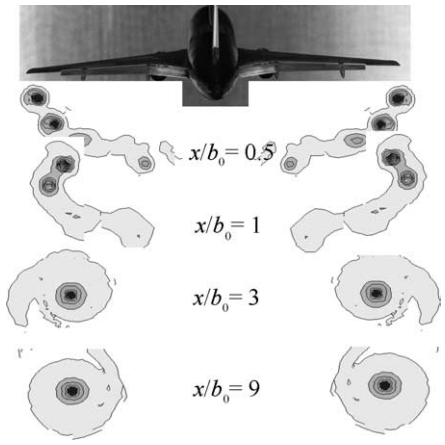

Fig. 1. Formation of a vortex pair downstream of a flapped aircraft model: iso-values of the longitudinal vorticity obtained by LDV in four different vertical planes downstream (b_0 denotes the model span, Crouch and Jacquin, 2005).

2. The stability of rotating 2D flows

Persistence of the trailing vortices is intriguing. It may be attributed to the stabilizing effects of rotation which are discussed in this section. It is well known that rotation may stabilize or destabilize a plane shear flow. It has been shown (see Sipp and Jacquin, 2000) that a steady 2D incompressible basic flow subject to rotation Ω is unstable if there exists a streamline for which, at each point:

$$2(V/\Re + \Omega)(W + 2\Omega) < 0, \tag{1}$$

where W is the vorticity of the streamline, $\Re$ its local algebraic radius of curvature and V the local norm of the velocity. $\Re > 0$ if the flow is locally counterclockwise and $\Re < 0$ if the flow is locally clockwise. Criterion (1) gives a sufficient condition of centrifugal instability. It actually generalizes a series of other criteria (see Sipp and Jacquin, 2000). If (1) is satisfied then the flow undergoes three-dimensional short-wave centrifugal-type instabilities. Note that two frame indifferent elements are involved in relation (1). These are the total vorticity ($W + 2\Omega$) and the total angular velocity ($V/\Re + \Omega$). Equivalence between rotation and streamline curvature lies in the latter term which groups the frame rotation Ω and the "curvature rotation" $V/\Re$.

Relation (1) may be used to evaluate the local stability of any curved flow fields. The underlying theory is an asymptotic development of the linearized Euler equations in the limit of very short-wave perturbations. This asymptotic method is scale independent and it describes also the production turbulence when it is applied to the mean streamlines of a turbulent flow (in this case, the underlying physics is identical to that of the rapid distortion theory of turbulence, see e.g. Cambon and Scott, 1999).

In the absence of frame rotation, relation (1) reduces to

$$2W \times V/\Re < 0. \tag{2}$$

Following this relation, a rectilinear shear flow ($|\Re| \to \infty$) is neutral (no centrifugal instability) and curvature destabilizes the flow when the sign of its vorticity is opposite to that of the curvature rotation. Applying this criterion to a 2D cylindrical flow gives the condition $\Phi(r) = 2W(r)V(r)/r < 0$ for instability, where $V(r)$ is now the orthoradial velocity, the vorticity being $W(r) = \mathrm{d}(rV)/r\,\mathrm{d}r$. This is the classical Rayleigh criterion for centrifugal instability (Rayleigh, 1916):

$$\sigma^2(r) = -\Phi(r) > 0. \tag{3}$$

$\Phi(r)$ is known as the Rayleigh discriminant and $\sigma(r)$ is the temporal amplification rate of the centrifugal instabilities. A fluid particle displaced in a flow region satisfying (3) will be expelled outward or inward due to an excess or a deficit of angular momentum $\Gamma(r) = rV(r)$. This enables for instance to make a clear distinction between a vortex, which verifies $\Gamma(r \to \infty) = \Gamma_0$, where Γ_0 is a constant, and a swirl, where $\Gamma(r \to \infty) = 0$. In the periphery of a swirl, angular momentum vanishes and the sign of vorticity W changes. Consequently, this flow is *always* unstable. In opposition, the angular momentum of an equilibrium 2D vortex is monotonous, so this flow is centrifugally stable. However, a vortex may be forced to become unstable through development of a local angular momentum (or circulation) overshoot. Examples will be given in the next section.

To conclude, a 2D vortex is a stable two-dimensional curved flow. Its non-viscous stability is a direct consequence of the monotonous distribution of its angular momentum. One must remind that the mechanisms of stabilization/destabilization by curvature or rotation which have been described in this section cannot be properly restored with a one- or two-equations turbulence model (they may only be mimicked by empirical corrections to these models). Full Reynolds stress closure models, which explicitly account for streamline curvature, are recommended. This is particularly important for computing flows containing trailing vortices (see e.g. Zeman, 1995).

3. The stability of a vortex

A model often used to fit experimental data is the Lamb–Oseen vortex:

$$V(r) = \frac{\Gamma_0}{2\pi r}(1 - \mathrm{e}^{-r^2/a^2}). \tag{4}$$

This is actually a solution of the 2D-Navier-Stokes equations, with a the vortex radius and $\Gamma_0 = \lim_{r\to\infty} 2\pi r V(r)$, the vortex circulation. The Reynolds number is $Re = \Gamma_0/\nu$. The flow (4) verifies $\Phi(r) \geqslant 0$. Following (3), this means that it is free from centrifugal instability.

Now, this vortex may become unstable if we add an axial flow. A canonical model in this case is the Batchelor vortex. The Batchelor vortex, or q-vortex, corresponds to the superposition of (4) with a Gaussian axial field:

$$U(r) = U_0 \pm \Delta U \mathrm{e}^{-(r/a)^2}. \tag{5}$$

The flow is controlled by the swirl number:

$$q = \frac{\Gamma_0}{2\pi a \Delta U} \approx 1.56 \frac{V_0}{\Delta U}, \tag{6}$$

where $V_0 = \max\{V\}$, and by the Reynolds number $Re = V_0 a/\nu$. Free trailing vortices are usually of the wake type, with sign '−' in (5), because they integrate the viscous losses along the mean streamlines. Stability properties of the Batchelor vortex have been extensively investigated (see Ash and Khorrami, 1995 for a review). Three families of instabilities have been identified. The first family are non-viscous short-wave instabilities due to stretching of vorticity perturbations aligned with the local shear. These instabilities are well described by the asymptotic study of Leibovich and Stewartson (1983) which leads to a necessary stability criterion generalizing (3). This criterion reads:

$$\sigma^2(r) = \frac{2V\left(r\frac{\mathrm{d}V}{\mathrm{d}r} - V\right)\left(\left(\frac{V}{r}\right)^2 - \left(\frac{\mathrm{d}V}{\mathrm{d}r}\right)^2 - \left(\frac{\mathrm{d}U}{\mathrm{d}r}\right)^2\right)}{\left(r\frac{\mathrm{d}V}{\mathrm{d}r} - V\right)^2 + \left(r\frac{\mathrm{d}U}{\mathrm{d}r}\right)^2} > 0. \tag{7}$$

The 2D criterion (3) is retrieved by putting $\mathrm{d}U/\mathrm{d}r = 0$ into (7). Distributions of σ^2 are shown in Fig. 2. When σ^2 is positive, the flow is locally unstable and σ corresponds to the temporal amplification rate of the instabilities. Fig. 2 shows that for $q = 1.5$ the core of the vortex is entirely stabilized ($\sigma^2 < 0$, $\forall r$); it is fully unstable ($\sigma^2 > 0$, $\forall r$) for $q = 0.7$. For intermediate values, e.g. $q = 1$, a stable buffer layer where $\sigma^2 < 0$ is surrounding the flow and prevents radial propagation of perturbations. The instability modes in the core take the form of "ring-modes" which exhibit a structure concentrated in an annular region located around the streamline where σ^2 is maximum. As said above, these modes develop for $q \leqslant 1.5$ and above this value the rotation transforms all the perturbations into neutral oscillations.

A second instability family is the viscous modes evidenced by Khorrami (see Ash and Khorrami, 1995). These modes occur for $q < 1.2$, and their growth rates are several orders of magnitude smaller than those of the inviscid modes occurring in this range. Consequently, they are unlikely to play any role in the dynamics of vortices. The third family is that of the viscous "centre-modes" recently described by Fabre and Jacquin (2004). These modes exist for any Reynolds numbers and swirl numbers, including $q > 1.5$. So they should be present in any trailing vortex. However, these modes are found to be concentrated in the very center of the vortex (Fabre and Jacquin, 2004). They could participate to a global "vortex meandering" of the vortex, but are probably unable to promote a turbulence diffusion of the vortex core.

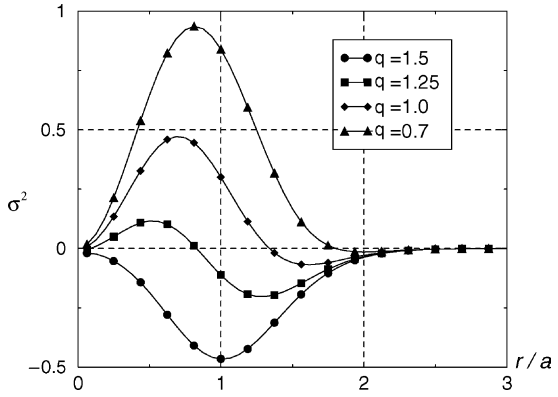

Fig. 2. Short-wave stability criterion for a Batchelor vortex: (squared) amplification factor as a function of the radius for different swirl number q (Jacquin and Pantano, 2002).

So, the inviscid short-wave instabilities described above (the "ring modes") are likely dominating the small scale dynamics of a 3D vortex. Indications on the non-linear development of these perturbations have been provided by direct numerical simulations (DNS). These DNS show that at the end of the linear regime, the perturbations saturate and decay without modifying significantly the vortex. This remarkable property was first described by Ragab and Sreedhar (1995). It is illustrated in Fig. 3 by results of Jacquin and Pantano (2002) who considered the case $q = 1$, $Re = V_0 a/\nu = 2000$. Fig. 3 shows the temporal evolution of the volume integral of the turbulence energy $k(r,t)$, $\langle k\rangle(t) = 2\pi \int_0^\infty rk(r,t)\,\mathrm{d}r$, and that of the swirl number $q(t)$ calculated using relation (6). Snapshots of vorticity are also shown. Quasi-random turbulence fluctuations were introduced initially. The results for the small times fit the stability theory (perturbations in Fig. 3(b) are ring modes and the slope of $\langle k\rangle(t)$ in the linear regime corresponds to the theoretical growth rate). At the saturation turbulence is filling the vortex. Later on, turbulence decays. The swirl $q(t)$ in Fig. 3(a) increases and cross $q = 1.5$. This indicates that the flow returns into a stable regime. Detailed results show that turbulent transport concentrate on the mean axial component of the velocity (decrease of ΔU), the tangential component V_0 being almost unchanged. The results of this anisotropic transport is an increase of $q(t)$ (Jacquin and Pantano, 2002).

An experiment which illustrates the above phenomenology but which also shows its limit is provided by Philips and Graham (1984). The experiment is based on the use of a split wing with a narrow central cylindrical body (see Fig. 4(a)). This apparatus produces a single vortex whose core may be manipulated by blowing a jet for instance. Fig. 4(b) and (c) shows radial profiles of the angular momentum (or circulation) rV. Fig. 4(b) corresponds to the case of a jet such that $q \approx 1.8$ (using (6)) in the first measurement section ($z/c = 45$). The flow verifies $q > 1.5$ so it is linearly stable (no ring mode). The measurements confirm that the vortex remains frozen downstream. However, when the jet becomes stronger, as in Fig. 4(c), one finds that $q \approx 0.4$ in the first measurement section ($z/c = 45$). Thus the flow is strongly unstable and it is subjected to a vigorous turbulent diffusion. The velocity excess ΔU quickly decays (not shown here) and the vortex core width a increases (note that at $z/c = 45$ the vortex width in Fig. 4(c) is already much larger that in the previous case). The non-viscous shear instabilities described above

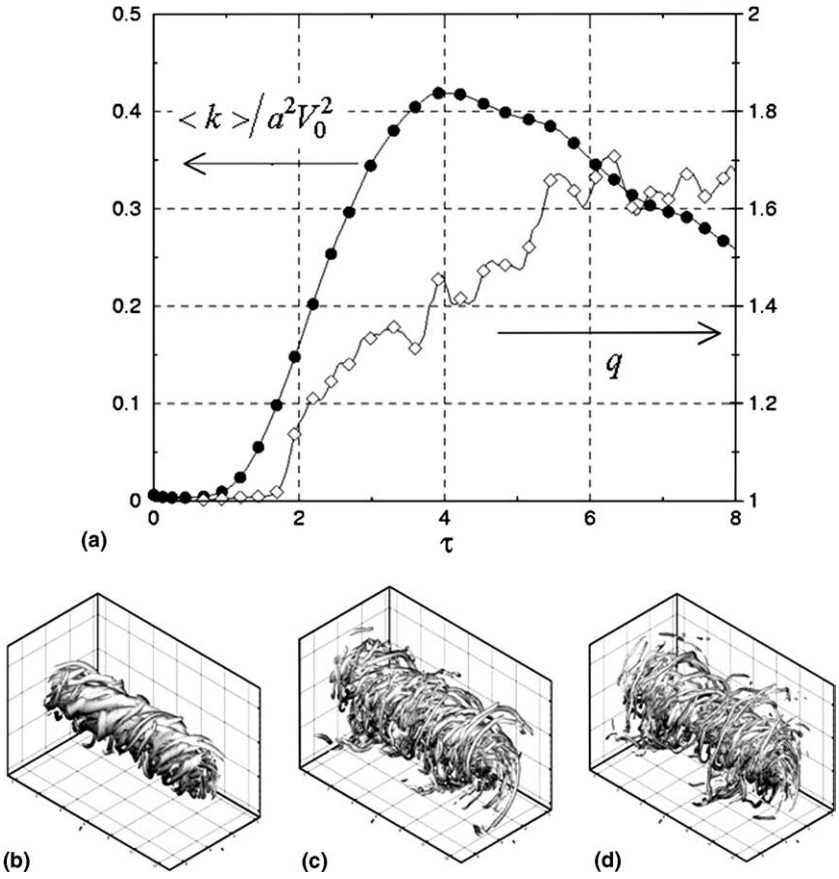

Fig. 3. DNS of a Batchelor vortex $q = 1$. (a) Volume integrated turbulent kinetic energy $\langle k \rangle$ and swirl number q versus time $\tau = tV_0/a_0$. Fluctuation of vorticity at $\tau = 1$ (b), $\tau = 2$ (c), and $\tau = 4$ (d) (Jacquin and Pantano, 2002).

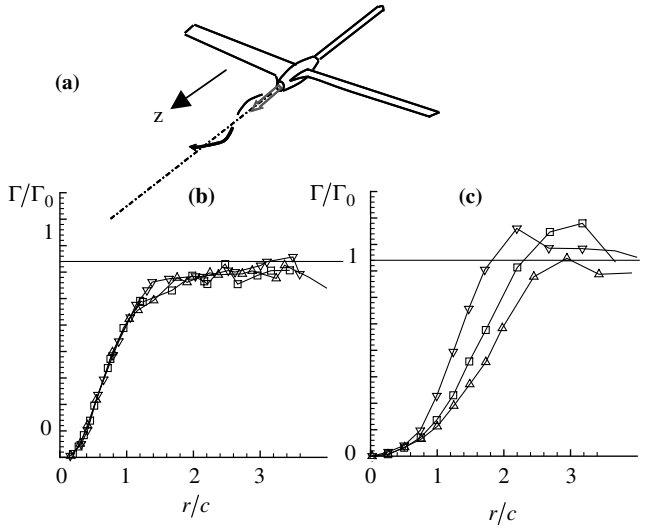

Fig. 4. Jet/vortex experiment: vortex generator with blowing capacity (a), circulation deduced from velocity measurements by hot wire in three downstream sections – case of a weak jet (b), case of a strong jet (c). Symbols: (▼) $z/c = 45$, (■) $z/c = 78$, (▲) $z/c = 109$ with c the wing chord length. Radius is normalized by c (Philips and Graham, 1984; Jacquin and Pantano, 2002).

(the "ring modes") are likely responsible of a strong radial transport of angular momentum and Fig. 4(c) shows that this leads to a large circulation overshoot. In the region where circulation decreases, the sign of vorticity changes and centrifugal instabilities develop in accordance with (3). The vortex width increases as the overshoot propagates radially. A small amplitude overshoot was already detected by Jacquin and Pantano (2002) in their DNS of the cases $q = 1$. These authors showed that this was due to a breaking of the stabilizing region which confines the perturbations within the core at higher swirl numbers (see Fig. 2). Note at last that a temporal DNS such as that of Fig. 3 is based on the supposition that the flow is statistically invariant along the flow axis. The rapid evolution of the flow for smaller q may invalidate this hypothesis. A spatial DNS would be required in this case.

To conclude, equilibrium vortices are likely stable and laminar. Their non-viscous stability may be asserted by application of available criteria and the viscous instabilities that have been detected seem too weak or too "singular". Even if we force it to be unstable, it goes back to a stable regime, except for large enough changes in the axial momentum (low enough swirl numbers). So, presumptions on the laminar nature of this flow are numerous, but unfortunately, it has never been possible to prove it without ambiguity by way of experiments. This is due to technical difficulties that will be commented in Section 7.

4. Vortex breakdown

Vortex breakdown is a phenomenon to which one often refers to when thinking about turbulence and vortices. Among available reviews on the topic, there are Délery (2001), Sarkpaya (1995) and Rusak and Wang (1996). Indeed, the physics of breakdown is completely different from that discussed above. It is related to the notion of criticality. As advocated by Benjamin (1962, 1967), vortex breakdown results from a transition from a globally stable and supercritical flow supporting only downstream travelling waves to a subcritical state supporting both upstream and downstream propagating waves. If the flow is subcritical, waves might transport energy upstream and disrupt the flow. As pointed by Gallaire and Chomaz (2003), this condition is close to an absolute/convective instability condition (a base flow is said to be absolutely or convectively unstable whether amplified disturbances increase in time at any fixed station and extend to the entire domain of interest or if such perturbations are transported downstream by the flow and if only the base flow remains for large time in any fixed frame). The complete phenomenon still escapes to our understanding. Experimental investigations of confined vortices in tubes (e.g. Tsai and Widnall, 1980) confirm that vortex breakdown represents a transition from a supercritical to a subcritical flow. This is also the case for the flow on a delta wing as illustrated below.

An important question indeed is the nature of the waves which propagate along the vortices and which may participate to breakdown. Any perturbation in a rotating flow leads to propagation of dispersive waves, called inertia waves. These waves are equivalent to the gravity waves found in stably stratified flows. Those which propagate in a vortex are named Kelvin waves and they play a fundamental role in the dynamics of vortices (see Saffman, 1992). The Kelvin waves in vortices have been extensively described theoretically by following a standard procedure which leads to linearize the Euler equations around a base flow considering modal small perturbations of the velocity and pressure of the type $(\underline{v}, p) = (\hat{\underline{v}}, \hat{p})(r)\mathrm{e}^{\mathrm{i}(kx+m\theta-\omega t)}$ where $\omega = \omega_r + \mathrm{i}\omega_i$ denotes a complex frequency, k is the axial wave number and m, the azimuthal wave number. This leads to an eigenvalue problem for ω. This problem admits a countable infinity of eigenvalues. A description of these waves is made in Saffman (1992) for a Rankine vortex (constant vorticity core). The case of the Lamb–Oseen vortex is detailed in Fabre et al. (in press). For the vortex breakdown we may restrict the analysis to axisymmetric modes $m = 0$ because they exhibit the largest propagation velocities (in the limit of small wave numbers). Results are shown in Fig. 5 for the Lamb–Oseen vortex. The eigenvalues are noted $\omega_{m,n}(k)$ where k and m are the axial and azimuthal wave numbers (here we consider $m = 0$) and where the absolute value of second index $|n|$ is related to the number of zeros of the eigenfunction (the higher the label, the more radial oscillations the mode contains). The sign of n is used to distinguish different families of waves. The frequencies

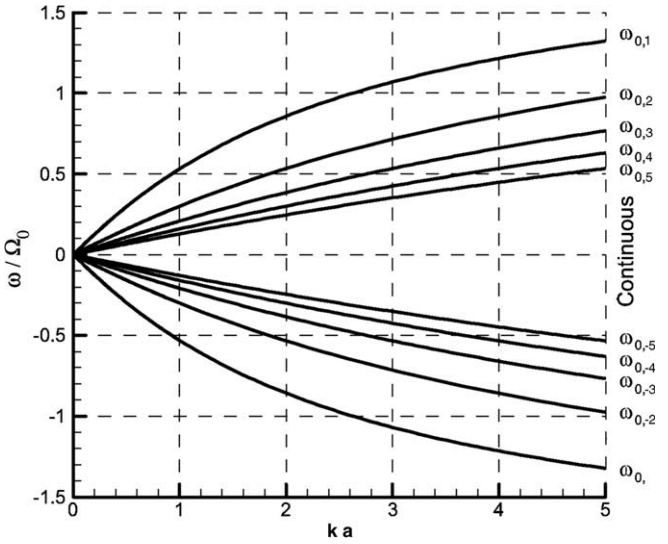

Fig. 5. Frequencies ω_r of the axisymmetric Kelvin waves in a Lamb–Oseen vortex. Frequencies are normalized by the vortex rotation rate $\Omega_0 = \Gamma_0/2\pi a^2$, where Γ_0 is the circulation, and a, the core radius (Fabre et al., in press).

are made non-dimensional with the rotation rate of the vortex center, $\Omega_0 = \Gamma_0/2\pi a^2$.

Axisymmetric Kelvin waves form two families of branches which propagate in opposite directions. The mechanism responsible for this propagation has been explained by Melander and Hussain (1994); and Arendt et al. (1997) (see also Fabre et al., in press). The group velocity $\mathrm{d}\omega_r/\mathrm{d}k$, which corresponds to the slope of the different branches, decreases with the wave number, the fastest waves being on the branch $\omega_{0,1}$ in the limit of long wavelength ($ka \to 0$). The group velocity of this wave is found to be $\mathrm{d}\omega_{0,1}(k)/\mathrm{d}k \approx 0.63\Gamma_0/(2\pi a)$ which is almost exactly equal to the maximum tangential velocity of the Lamb–Oseen vortex. This means that energy of perturbations propagates with a speed smaller but close to the maximum tangential velocity of the vortex, $\mathrm{d}\omega_{0,n}(k)/\mathrm{d}k < V_0$, a property which also holds for other vortex models. This is sufficient to understand that occurrence of breakdown needs a tangential velocity component comparable to the axial component. As an illustration, Fig. 6(a) shows an hydraulic visualization of the phenomenon on a delta wing with a swept angle $\varphi = 60°$ at incidence $\alpha = 20°$ (Werlé, 1982). Fig. 6(b) and (c) show the velocity component parallel to the vortex axis measured by LDV on a delta wing with 70° swept angle at 30° of incidence in a wind tunnel (Mitchell and Délery, 2001). Criticality is illustrated by Fig. 6(d) and (e) which depict the axisymmetric Kelvin waves deduced from a temporal stability analysis of the base flow $(U, V)(r)$ obtained from an azimuthal averaging of the data of figures (b) and (c) (Renac, 2004). Compared to Fig. 5, the axial flow leads to a Doppler shift of the waves (in the simple case of a uniform convection at velocity U_∞, ω_r/k is transformed into $\omega_r/k + U_\infty$). Upstream of the breakdown location, the flow is supercritical (all

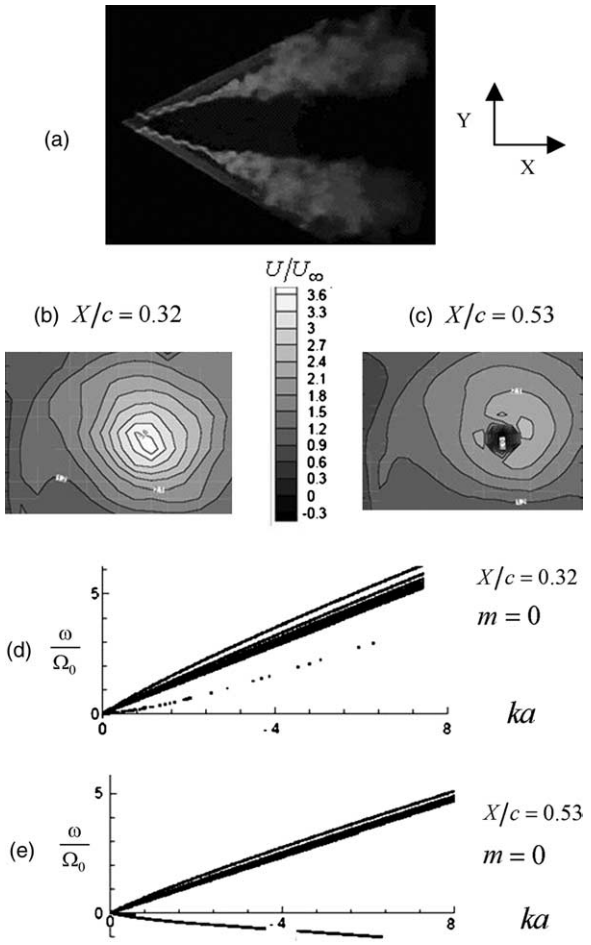

Fig. 6. Vortex bursting on a delta-wing. (a) Hydraulic visualization on a wing with a swept angle $\varphi = 60°$ and an incidence $\alpha = 20°$ (a) (Werlé, 1982). (b, c) Axial component U of the mean axial velocity normalized by the free-stream velocity U_∞, measured by LDV in a vortex over a delta wing with $\varphi = 70°$ and $\alpha = 30°$ for $Re = U_\infty c/\nu = 1.5 \times 10^6$ in two vertical planes, $X/c = 0.32$ and $X/c = 0.53$, the busting being located at $X/c = 0.41$, with c the wing chord length (Mitchell and Délery, 2001). (d, e) Axisymmetric Kelvin waves obtained by a linear analysis of the velocity field $(U, V)(r)$ deduced from azimuthal averaging of the LDV results of figures (b, c) (Renac, 2004).

branches of Fig. 6(d) have a positive slope); downstream, the flow is subcritical (presence of negative slopes in Fig. 6(e)).

A crude criterion for breakdown thus amounts to consider that the fastest waves travel at a speed $c \approx V_0$. Criticality then leads to consider the following non-dimensional parameter:

$$q_c = \frac{V_0}{U_\infty + \Delta U} = \frac{q}{1.56} \frac{1}{1 + U_\infty/\Delta U}, \tag{8}$$

where q is defined in (6). The flow remains supercritical (free from breakdown) if q_c is smaller than unity. The second identity shows that a supercritical vortex ($q_c < 1$) may remain locally stable with respect to short-wave inviscid instabilities ($q \geqslant 1.5$) thanks to the drift velocity U_∞ in (8). By approximating the maximum tangential velocity by $V_0 \approx \Gamma_0/(2\pi a)$ one notes that given the circulation Γ_0, bursting condition critically depends on the core width a. This may be used to get an estimation of core width minimums. In the case of the vortices on a delta wing one may consider $\Gamma_0 = U_\infty \sin\alpha \times s(X)$ with $s(X) = 2X/\tan\varphi$ the local span of the delta wing (φ is the swept angle). The first equality in relation (8) leads to

$$q_c = \frac{\sin\alpha}{2\pi} \frac{s(X)}{a} \frac{U_\infty}{U_\infty + \Delta U}. \tag{9}$$

For the data of Fig. 6(b) we have $X/c = 0.32$, $\Delta U/U_\infty = 2.6$, so that $a/s(X) \geqslant 0.03$ for $q_c \leqslant 1$: the vortex core width in the supercritical region (before breakdown) is only few percent of the span. An order of magnitude may be also obtained for the trailing vortices behind a wing by using for the load the elliptic law $\Gamma_0 = 2C_z U_0 b_0/(\pi AR)$ (see any text books on aerodynamics) where C_z is the lift coefficient, AR, the wing aspect ratio, b_0, the wing span. Typical values for a highly loaded wing (aircraft in landing configuration) are $AR = 7$, $C_z = 2$. With this choice the trailing vortices are free from breakdown ($q_c \leqslant 1$) if $a/b_0 \geqslant 0.03 U_\infty/(U_\infty + \Delta U)$. As trailing vortices are usually of the wake type ($\Delta U < 0$), $a/b_0 = 3\%$ must be considered as a minimum for a trailing wake vortex with no bursting. This is compatible with known data.

So vortex breakdown is a global instability mechanism by opposition to the local instabilities considered in the previous sections. Occurrence of a breakdown may be associated to possible propagation against the current of inertial waves. Equilibrium trailing vortices are free form breakdown (vortices on a delta wing are not "trailing vortices") and this imposes a minimum value to their core width.

5. The stability of vortex systems

Vortices in interaction are generally unstable with respect to 3D perturbations. This will be explained now. Two kinds of instabilities, referred to as 'cooperative instabilities', are known to occur in vortex systems. The first kind is characterized by long wavelengths, typically of the order of the distances between the different vortices of the wake. The most famous long-wave instability is the Crow instability occurring in a pair of counter-rotating vortices (Crow, 1970). Other forms of long-wave instabilities occurring in multipolar wakes were also considered (Crouch, 1997; Fabre et al., 2002), and may be investigated using a vortex filament method described below. Long-wave instabilities do not saturate and generally lead to a reconnection of the different vortices. The second kind of cooperative instabilities are characterized by short wavelengths, typically of the order of the vortex core radii. This kind of instability was discovered simultaneously by Moore and Saffman (1975) and Tsai and Widnall (1976). These instabilities are expected to play an important role in the mechanism of merging between co-rotating vortices (Le Dizes and Laporte, 2002). These two types of instabilities will be detailed now.

When separations between the vortices are large compared with their thickness and if we consider long wave perturbations, a system of stability equations may be derived by considering a set of parallel vortex filaments with slight sinusoidal perturbations of their respective positions (see Crow, 1970; Crouch, 1997; Fabre et al., 2002). The system evolves due to superposition of three effects: (i) the straining experienced by each filament when displaced by a perturbation from its mean position in the velocity field induced by the other undisturbed filaments, (ii) the self induced rotation of the disturbed filament and (iii) the velocity field induced on the filament by the other vortices when they are themselves perturbed from their mean positions. Mechanism (i) is schematized in Fig. 7(a) and (b) for the particular case of a pair of counter-rotating vortices. It leads to amplification of the perturbations whose polarization planes remain close to the extension planes of the straining field. This mechanism is in balance with the self-induction, mechanism (ii), which tends to shift away the perturbation from these planes; as schematized in Fig. 7(c), the Biot–Savart velocity field induced by the vortex on itself, when it is sinusoidally displaced by mechanism (i), leads to rotation of the vortex around its mean axis in a direction opposite to that of the vortex core. One may also explain this self induction effect as the result of the propagation of particular asymmetric Kelvin modes $m = \pm 1$ (see e.g. Fabre et al., 2002), so that this mechanism introduces a dependence of the solution with respect to a measure of the vortex core radius.

A first example of long-wave instabilities in a vortex system is the Crow instability already mentioned. The Crow instability develops in pairs of counter-rotating vortices of circulation $\pm\Gamma_0$. Its characteristic time scale is $\tau \approx 2\pi b^2/|\Gamma_0|$ (actually the inverse of the strain rate) with b the vortex separation. It is responsible of the deformation and break-up of aircraft contrails (see Fig. 8). A second example of long-wave instabilities is shown in Fig. 9. This corresponds to long-wave perturbations which develop in the vortex system composed with two vortex pairs of opposite signs, as sketched in Fig. 9(a). The vortex pairs may be co-rotating ($\Gamma_1 > 0$, $\Gamma_2 > 0$) or counter-rotating ($\Gamma_1 > 0$, $\Gamma_2 < 0$). This vortex configuration is used to model the vortex wake of aircrafts: the outer vortex pair is that produced at the wing tips and the inner one, by flaps and horizontal tail planes. This problem has been recently investigated in the context of researches on aircraft wake hazard alleviation. The solution of the linear problem depends on Γ_2/Γ_1 and on b_2/b_1. Fig. 9(b)–(e) shows, for the case ($\Gamma_2/\Gamma_1 = -0.3$, $b_2/b_1 = 0.3$), the most amplified perturbation at four different instants during one revolution of the inner vortices around the outer ones. The amplification factor of this perturbation is much larger than that of the Crow instability obtained without the inner vortices. The towing tank result shown in Fig. 9(f) confirms that this type of perturbation is effectively selected in a real four vortex wake (see Bristol et al., 2004). Differences between the linear solution Fig. 9(e), and the experiment, Fig. 9(f), are the bending of the loops and burstings. These phenomena are due to non-linearity. A premature break-up of aircraft trailing vortices could be obtained by promoting this kind of instabilities (see Crouch and Jacquin, 2005).

Let us consider now the short-wave instabilities. This kind of instabilities results from the stretching of perturbations whose wavelengths are of the order of the vortex core radii. Fig. 10 shows results of a direct numerical simulation of a co-rotating dipole of aspect ratio $a/b = 0.2$ for $Re = 5000$ (Le Dizes and Laporte, 2002). Contrary to the case of the counter-rotating vortex pair schematized in Fig. 7, the strain is now rotating with the pair. Fig. 10(a) shows the linear development of the short-wave perturbation. For $a/b = 0.2$ the vortices are sufficiently close to exchange their vorticity and this leads to the merger (see Fig. 10(b)).

A very different example of flow involving short-wave cooperative instabilities is shown in Fig. 11. This is a

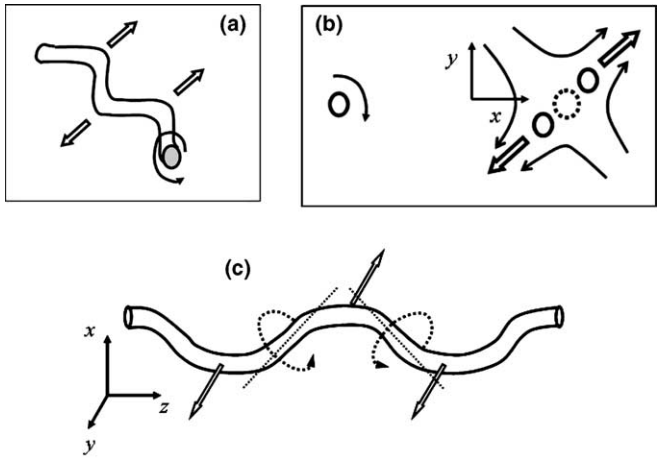

Fig. 7. Amplification of a deformed vortex by the strain in a pair of two counter-rotating vortices of same strength: (a) side view, (b) front view. (c) Self-induced rotation of a sinusoidally displaced vortex in a plane $y = 0$: due to the curvature, the Biot–Savart velocity induced by the two vortex sections normal to the two dotted lines, for instance, leads to displacements of the vortex along directions $\pm y$ normal to the perturbed vortex plane as indicated by the straight arrows. Note that the resulting self induced rotation is opposite to the vortex core rotation.

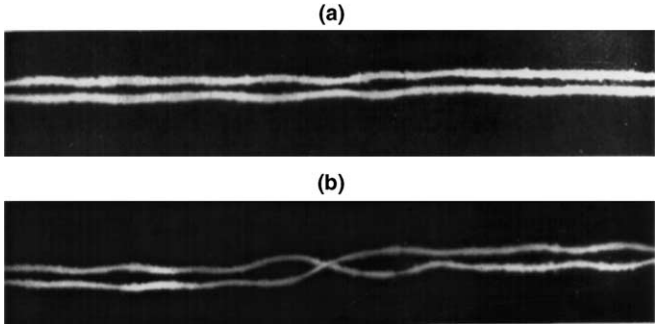

Fig. 8. Development of the Crow instability in a contrail at two different instants (Crow, 1970).

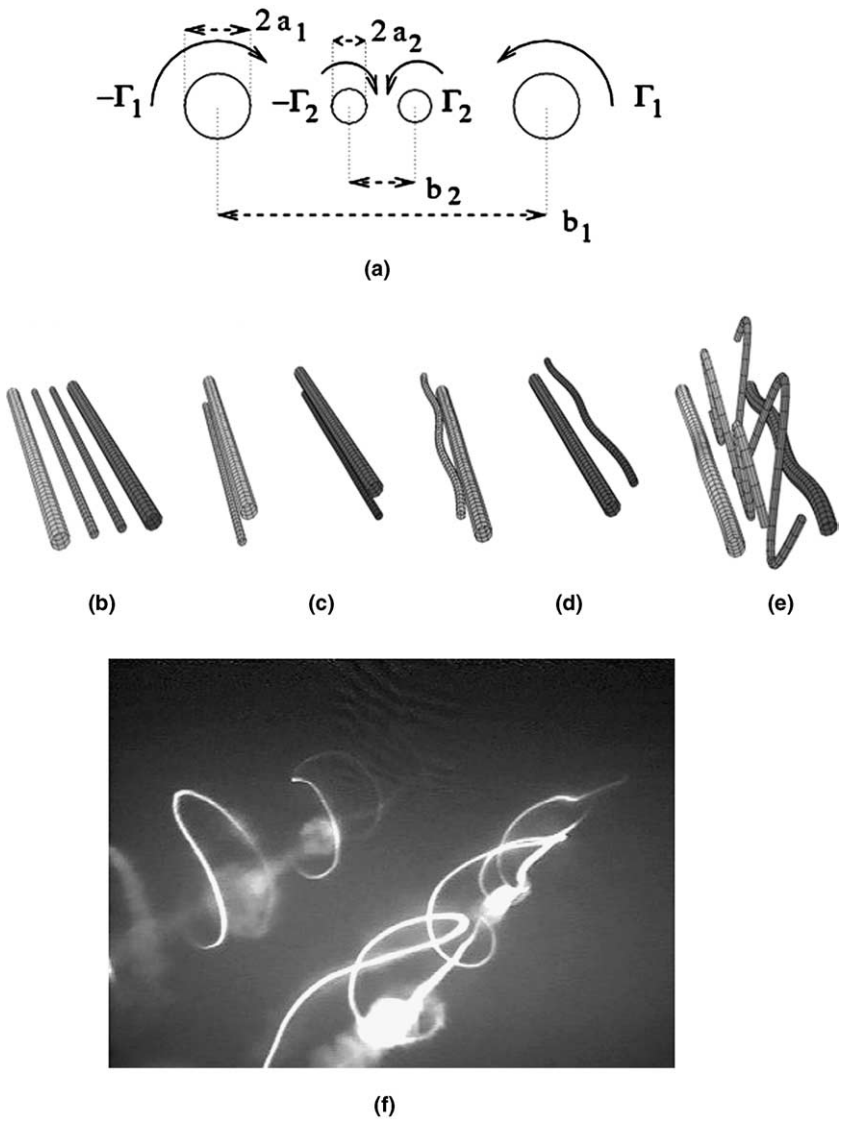

Fig. 9. Long-wave cooperative perturbation in a four-vortex system idealizing the wake of a wing equipped with flaps: (a) definitions of the four-vortex system, (b–e) optimal perturbation obtained with the linear theory after one revolution of the inner vortex pair around the outer one (case $\Gamma_2/\Gamma_1 = -0.3$, $b_2/b_1 = 0.3$, Fabre et al., 2002), (f) towing tank experiment for $\Gamma_2/\Gamma_1 = -0.37$, $b_2/b_1 = 0.5$ (Bristol et al., 2004). (f) Shows the perturbation which develops after an elapsed time close to that corresponding to (e).

mixing layer developing over a cavity at transonic regime (see Forestier et al., 2003). In such a flow, an aero-acoustic resonance leads to development of well defined 2D spanwise vortices visible on the Schlieren picture in Fig. 11(b). Thanks to the periodic nature of the flow, the velocity field may be described by means of a conditional analysis (see Fig. 11(c) and (d)). Looking to the random fluctuations which are superposed to this coherent phase-averaged field and which characterize small scale activity, one finds that it develops in the centre of the vortices, see Fig. 11(d). This is likely due to short-wave instabilities which develop in the cores of the co-rotating vortices subjected to a mutual straining (this straining is responsible for the elliptic shape of the streamlines shown in Fig. 11(c)). Contrary to Fig. 10, here, the vortices hit the downstream corner of the cavity before the instability has time to grow sufficiently. In that case, the vortices do not merge and an aero-acoustic loop takes place.

To conclude, mutual straining of vortices may lead to their rapid disorganization thanks to the development of long-wave perturbations with wavelengths of the order of the vortex separation. Perturbations with wavelengths of the order of the vortex core radii also develop on the same time scale. The long-waves may quickly put the vortices in contact and the short-waves are responsible for the merger phenomenon.

6. Density effects in vortices

In a rotating flow, centripetal acceleration plays the same role as gravity in standard buoyancy problem. Consequently, density variations in vortices may be a source of

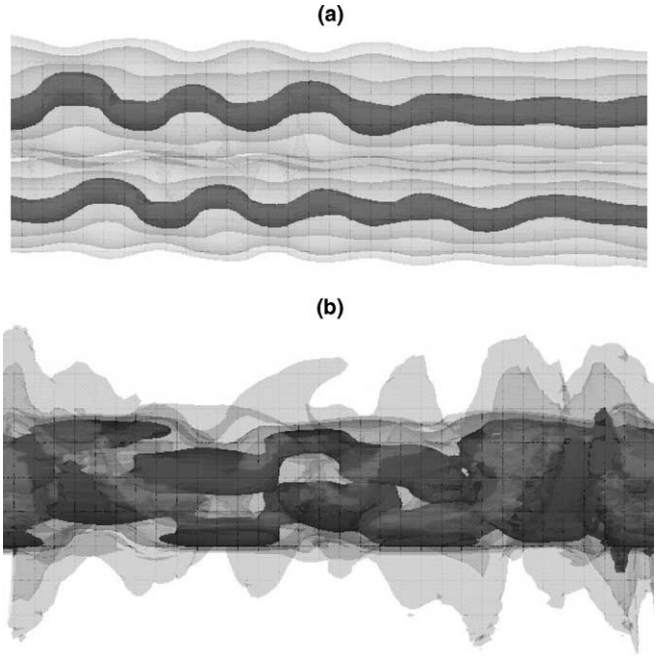

Fig. 10. Iso-levels of the axial vorticity perturbation component in a direct numerical simulation of a co-rotating dipole of aspect ratio $a/b = 0.2$ for $Re = 5000$: (a) linear regime, (b) merger (Le Dizes and Laporte, 2002).

instabilities. This problem will be briefly commented here. Fig. 12(a) depicts the analogy between an unstable non-homogeneous shear flow under the action of gravity and an unstable non-homogeneous swirling flow. It shows that a heavy vortex core is unstable with respect to 2D perturbations whereas a light one is stable. The stability of non-homogeneous vortices have been investigated by several authors, see a review in Sipp et al. (2005). Important quantities are the Rayleigh discriminant, already introduced in (3), and the parameter:

$$G^2 = -\frac{V^2}{r}\frac{1}{\rho}\frac{\mathrm{d}\rho}{\mathrm{d}r}$$

which corresponds, if $\mathrm{d}\rho/\mathrm{d}r > 0$, to the square of a buoyancy frequency, and which is analogous to the classical buoyancy frequency (or Brunt–Väisälä frequency), but with gravity replaced by the centrifugal acceleration V^2/r. A critical value for this frequency is $G_w^2 = \frac{r}{4}\frac{\mathrm{d}V/r}{\mathrm{d}r}$ (critical Richardson number). Fig. 12(b) gives an overview of the different type of instabilities which have been identified for different values of G^2. This graph is given here to illustrate the great complexity of this problem. The details are given in Sipp et al. (2005). The regime $G^2 > 0$ is particularly interesting because it corresponds to vortices which are stable ($\Phi > 0$) in the absence of density gradient. When density is larger in the core, Rayleigh–Taylor (RT) instabilities develop and may compete with centrifugal instabilities. The RT instability mainly affects non-axisymmetric two-dimensional eigenmodes (see Sipp et al., 2005). As we did in the case of the Batchelor vortex in Section 3, it is interesting to look the non-linear regime of these instabilities. DNS of a Lamb–Ossen vortex with a heavy core dominated by RT

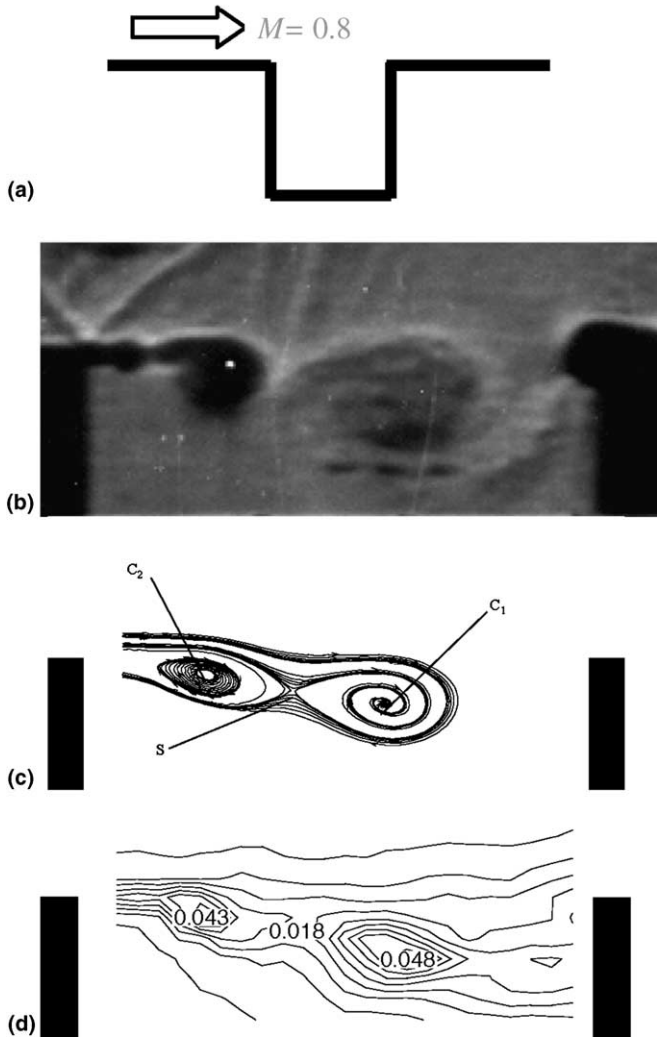

Fig. 11. The mixing layer over a cavity at transonic regime: (a) schematic, (b) Schlieren picture of the mixing layer, (c) pseudo streamlines deduced from a conditional analysis of LDV measurements, (d) iso-levels of the variance of the random part of the fluctuating field (component $\langle u'^2\rangle/U_\infty^2$). Note that these fluctuations develops in the vortex core; this is likely due to short-wave instabilities (Forestier et al., 2003).

instabilities has been performed by Coquart et al. (2005). It shows that these instabilities quickly saturate and leave the mean vortex almost unchanged. This is illustrated in Fig. 13. The case corresponds to a Lamb–Ossen vortex at a Reynolds number $Re = V_0 a/\nu = 10{,}000$ with a Gaussian density distribution in its centre (see Fig. 13(a)). The density on the axis is increased by 20% with respect to the density outside the vortex. The most amplified perturbation is a $m = 3$ RT mode (see Fig. 13(a)). In Fig. 13(b), we enter the non-linear regime: the flow exhibits the mushroom-like patterns characteristic of the non-linear development of the RT instability (Clark, 2003). In the late stage development of the instability, these patterns are stretched in the azimuthal direction and subject to filamentation. Fig. 13(e) shows that, contrary to flows where RT instabilities are due to gravity, the stretching effects in the vortex quickly damp the cascade of instabilities. The density perturbations

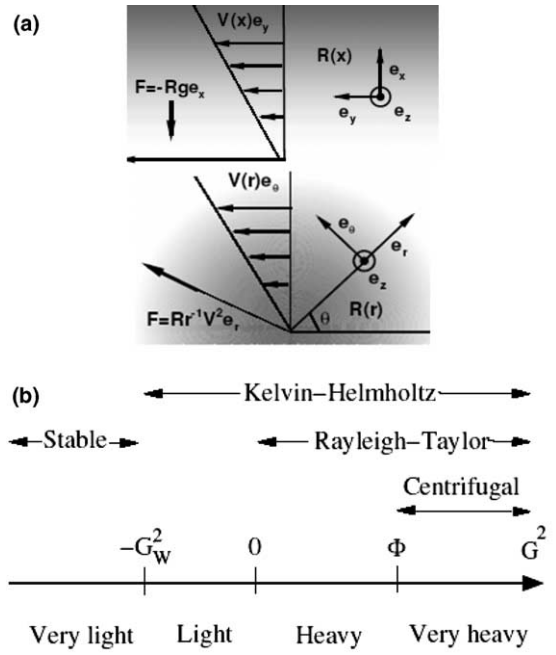

Fig. 12. (a) Analogy between unstable non-homogeneous shear flow under the action of gravity (upper figure) and unstable non-homogeneous swirling flow (lower figure). The grey levels sketch the density field which is noted R. (b) overview of instabilities in the case where $\Phi(r) > 0$ (see text for the definition of the parameters, Sipp et al., 2005).

quickly dies out (see Fig. 13(e)) letting the vortex almost unchanged (see Fig. 13(f)). Density variations effectively destabilize a vortex, but the instabilities quickly saturate and the density contrast is rapidly eliminated. The vortex itself remains almost unaffected. Even if a lot remains to do on this interesting subject the above results bring an additional illustration of the persistence of vortices.

7. Measurement limitations

This is not easy to characterize vortices experimentally. Conventional velocimetry techniques (LDV, PIV, hot-wire) should nominally operate in a three-component mode in order to characterize the dynamics discussed above. Such measurements must provide axial and tangential mean velocity profiles, lengthscales (core radii, vortex separations), variances of the velocity, power spectral densities and, possibly, other two-point statistics. The difficulties come from the small size of the vortices produced in the laboratory and from their unsteady nature. These two aspects are briefly discussed here.

Fig. 14(a) shows the structure of the vortices of Fig. 1 at $x/b_0 = 5$. The figure depicts the tangential velocity V (actually a cylindrical averaging of LDV measurements) for two configurations, the flapped case shown in Fig. 1 and a clean case (no flap). The lift coefficients are, respectively, $C_z = 1.7$ and $C_z = 0.7$. The free-stream velocity is $V_\infty = 50\ \mathrm{m\ s^{-1}}$ and the Reynolds number based on the aerodynamic chord ($c \approx 66$ mm) is $Re_c = 220{,}000$. Transition was tripped on the wings and on the fuselage. The properties of these profiles are detailed in Jacquin et al. (2003). One must note here is that the "internal core" (or "viscous core") rotating as a

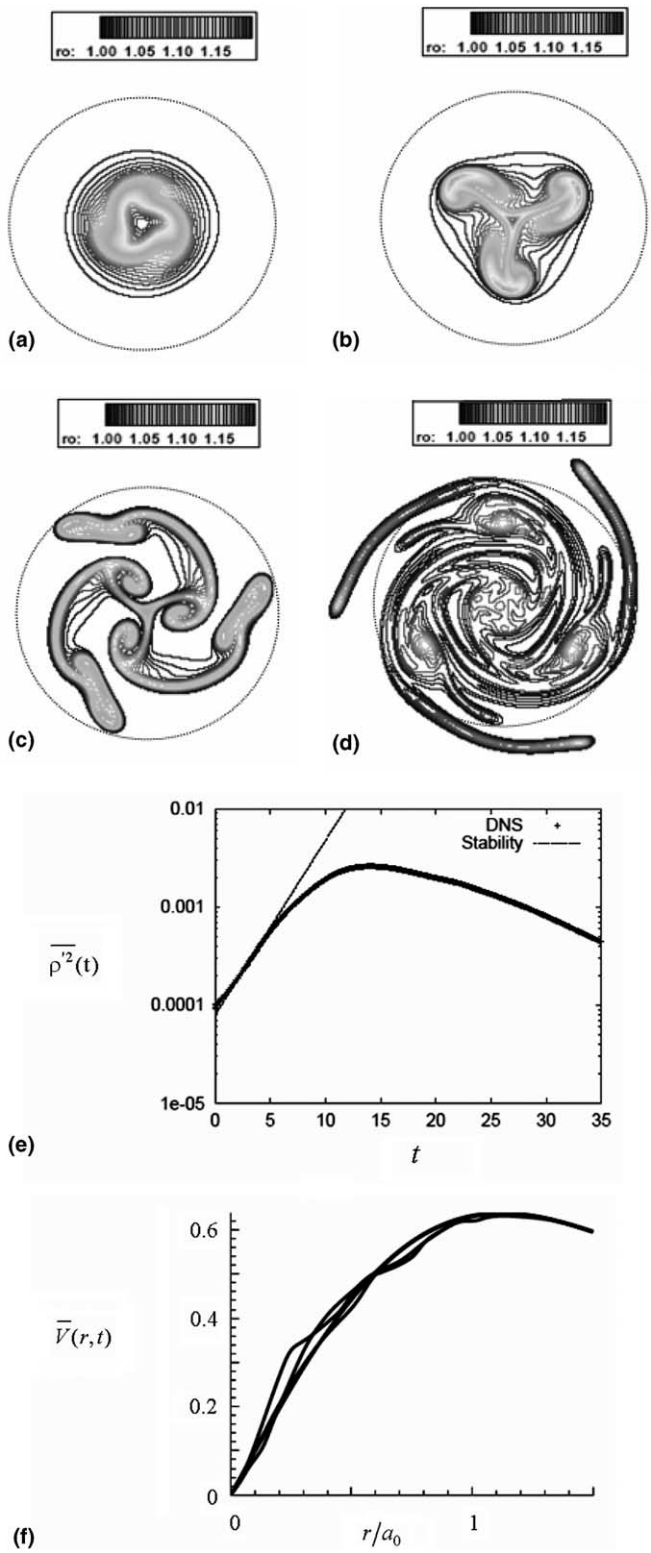

Fig. 13. Density $\rho(r,\theta,t)$ at different times: (a) $t = 0.16$, (b) $t = 11$, (c) $t = 20.4$, (d) $t = 34.5$, (e) variance of the density perturbation $\overline{\rho'^2}(t)$ as a function of time t; (f) tangential velocity $\overline{V}(r,t)$ as a function of the radius r for times corresponding to (a–d). The bar denotes an average in the axial direction. The circle in (a–d) corresponds to the vortex radius (Coquart et al., 2005).

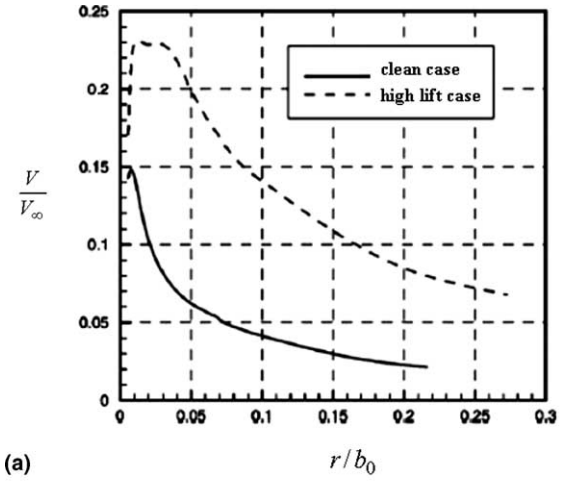

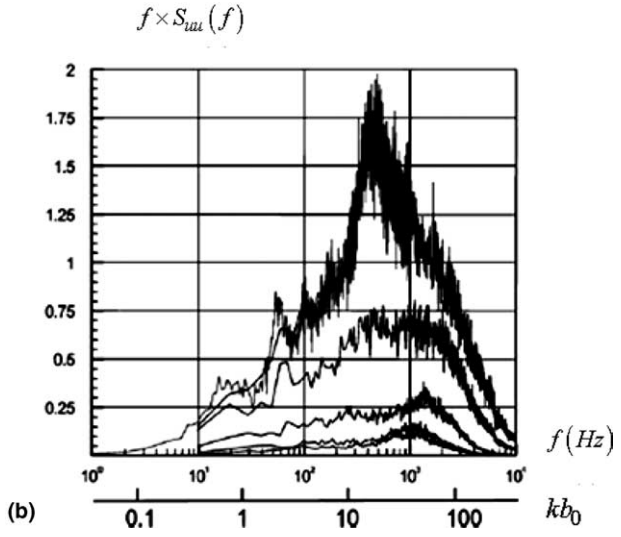

Fig. 14. (a) Tangential velocity V/V_∞ as a function of radius measured at $x/b_0 = 5$ in the left hand vortex of the model of Fig. 1, in a clean and high-lift configurations (Jacquin et al., 2003). (b) Power density spectra of the longitudinal velocity component obtained by translating a hot wire along a vertical line in the vortex of the high lift case shown in Fig. 1. The power spectra are multiplied by the frequency. The highest energy is obtained on the vortex axis. Each curve corresponds to a displacement of $\Delta z = 1$ mm ($\Delta z/b_0 \approx 2 \times 10^{-3}$) with respect to the vortex axis.

solid body is very narrow, less than 1% of the span b_0. It is too small for instance to be described by the measurement system (here a 3D LDV system, see Jacquin et al., 2003). As for the velocity fluctuations, it is found that their energy reaches its maximum in the center of the vortex. This is illustrated in Fig. 14(b) which shows the power spectral density of the axial component of the velocity measured with a standard single wire probe displaced in the core of the high lift vortex of Fig. 14(a). Energy is maximum when the hot wire is in the centre. A small displacement from this position leads to a sharp decrease of the energy. The same is found in many vortices and this is not turbulence. Fig. 14(b) is characterizing a global meandering of the vortex. It turns out that vortices produced in experiments are never steady: even when separation with other vortices is sufficiently large

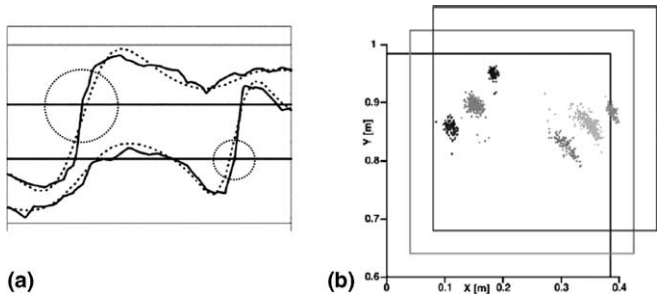

Fig. 15. Characterization by PIV of vortex unsteadiness of two vortices generated by flap and tip of a flapped wing: (a) two horizontal profiles of the vertical velocity component from cuts in PIV results (solid lines) and their approximations by the superposition of two Lamb–Oseen vortices (dashed lines; the dotted circles materialize the Lamb–Oseen vortices, their radius being proportional to the vortex radius a, see (4)), (b) distribution of vortex centre points deduced from the approximation by two Lamb–Oseen vortices (centres of the circles of (a)). The three different frames (shifted one from the other) refer to different configurations of the same model (using, respectively, 95, 298 and 100 PIV samples) in the same region of the flow. The clusters on the left and right hand sides of each frame correspond, respectively, to the wing tip and flap tip vortices (Vollmers, 2001).

and axial flow sufficiently weak for discarding the main instability mechanisms discussed previously, one observes that vortices are always subjected to random displacements of small amplitudes. These are the random variations of the mean field of Fig. 14(a) ahead of the fixed probe which lead to Fig. 14(b). Vortex meandering is a universal phenomenon which is still not understood. The first comprehensive investigation of this problem is due to Devenport et al. (1996). Meandering could result from a superposition of several mechanisms as discussed in Jacquin et al. (2003). Fortunately, there are cases where the source of fluctuations may be readily attributed to instability mechanisms described above. An example is provided in Fig. 15, where the variations in the position of the vortices deduced from PIV measurements exhibit a preferential orientation which may be attributed, without ambiguity, to a cooperative instability (see Vollmers, 2001).

8. Conclusions

The dynamics of trailing vortices has been discussed on the basis of recent findings. Some important mechanisms have been recalled and are recapitulated below.

- Rotating flows may be stabilized or destabilized. Theoretical works based on asymptotic linear methods have provided useful stability criteria.
- An equilibrium trailing vortex is free from non-viscous instabilities. Viscous instabilities have been detected but they are weak or confined in the very centre of the vortices.
- Non-viscous instabilities may be forced if we introduce a jet or a wake. But these instabilities are usually transient and decay quickly without modifying the vortex significantly.

- The above results are suggesting that trailing vortex are laminar.
- Significant change must be however obtained when the jet (or wake) is strong enough. In this case, the vortex is subjected to a rapid diffusion thanks to propagation of a front of centrifugal instabilities (circulation overshoot).
- Vortex systems are subjected to cooperative instabilities. Long-wave instabilities may lead to break-up of the system and short-waves instabilities participate to the merger of the vortices.
- Density variations in the core may lead to Rayleigh–Taylor type instabilities. Available results show that, again, this instability quickly saturates and does not affect the vortex.
- Trailing vortices in the laboratory have very narrow cores.
- Large gradients and a general meandering of these structures make their experimental characterization particularly difficult.

Acknowledgements

The author is indebted to his outstanding students, Denis Sipp, David Fabre, Carlos Pantano, Nicolas Forestier, Florent Renac and Laure Coquart for their contributions to the matter presented in this paper. He warmly thanks Jean Paul Bonnet, from University of Poitiers, and all the members of the organizing comity of EXHFT6, for their kind invitation to make a presentation of this review in Japan.

References

Arendt, S., Fritts, D.C., Andreassen, O., 1997. The initial value problem for Kelvin vortex waves. J. Fluid Mech. 244, 181–212.

Ash, R.L., Khorrami, M.R., 1995. Vortex stability. In: Green, S.I. (Ed.), Fluid Vortices, Fluid Mechanics and Its Applications, vol. 30. Kluwer Academic Publishers, pp. 317–372.

Benjamin, T.B., 1962. Theory of the vortex breakdown phenomenon. J. Fluid Mech. 14 (4), 593–629.

Benjamin, T.B., 1967. Some developments in the theory of vortex breakdown. J. Fluid Mech. 28 (1), 65–84.

Bristol, R.L., Ortega, J.M., Marcus, P.S., Savas, O., 2004. On cooperative instabilities of parallel vortex pairs. J. Fluid Mech. 517, 331–358.

Cambon, C., Scott, J.F., 1999. Linear and nonlinear models of anisotropic turbulence. Annu. Rev. Fluid Mech. 31, 1.

Clark, T.T., 2003. A numerical study of the statistics of a two-dimensional Rayleigh–Taylor mixing layer. Phys. Fluids 15, 2413.

Coquart, L., Sipp, D., Jacquin, L., 2005. Mixing induced by Rayleigh–Taylor instability in a vortex. Phys. Fluids, 17.

Crouch, J.D., 1997. Instability and transient growth for two trailing vortex pairs. J. Fluid Mech. 350, 311–330.

Crouch, J., Jacquin, L. (Eds.), 2005. Aircraft Trailing Vortices. C.R. Physique 6 (4–5).

Crow, S.C., 1970. Stability theory for a pair of trailing vortices. AIAA J. 8 (12), 2172–2179.

Délery, J., 2001. Aspects of vortex breakdown. Prog. Aerospace Sci. 30, 1–59.

Devenport, W.J., Rife, M.C., Liaps, S.I., Follin, G.J., 1996. The structure and development of a wing tip vortex. J. Fluid Mech. 312, 67–106.

Fabre, D., Jacquin, L., 2004. Viscous instabilities in trailing vortices at large swirl numbers. J. Fluid Mech. 500, 239–262.

Fabre, D., Jacquin, L., Loof, A., 2002. Optimal perturbations in a four-vortex aircraft wake in counter-rotating configuration. J. Fluid Mech. 451, 319–328.

Fabre, D., Sipp, D., Jacquin, L., The Kelvin waves of the Lamb–Oseen vortex. J. Fluid. Mech., in press.

Forestier, N., Jacquin, L., Geffroy, P., 2003. The mixing layer over a deep cavity in a transonic regime. J. Fluid Mech. 475, 101–145.

Gallaire, F., Chomaz, J.M., 2003. Mode selection in swirling jet experiments: a linear stability analysis. J. Fluid Mech. 494, 223–253.

Jacquin, L., Pantano, C., 2002. On the persistence of trailing vortices. J. Fluid Mech. 471, 159–168.

Jacquin, L., Fabre, D., Sipp, D., Vollmers, H., Theofilis, V., 2003. Instability and unsteadiness of aircraft vortex wakes. Aeronaut. Sci. Technol. 7 (8), 577–593.

Le Dizes, S., Laporte, F., 2002. Theoretical prediction of the elliptic instability in two vortex flow. J. Fluid Mech. 471, 169–201.

Leibovich, S., Stewartson, K., 1983. A sufficient condition for the instability of columnar vortices. J. Fluid Mech. 126, 335–356.

Melander, M.V., Hussain, F., 1994. Core dynamics on a vortex column. Fluid. Dyn. Res. 13, 1–37.

Mitchell, A.M., Délery, J., 2001. Research into vortex breakdown control. Prog. Aerospace Sci., 385–418.

Moore, D.W., Saffman, P.G., 1975. The instability of a straight vortex filament in a strain field. Proc. R. Soc. London Ser. (A) 346, 413–425.

Philips, W.R.C., Graham, J.A.H., 1984. Reynolds stress measurements in a turbulent trailing vortex. J. Fluid Mech. 47, 353–371.

Ragab, S., Sreedhar, M., 1995. Numerical simulations of vortices with axial velocity deficits. Phys. Fluids 7, 549–558.

Rayleigh, J.W.S., 1916. On the dynamics of revolving flows. Proc. R. Soc. London Ser. A 93, 148.

Renac, F., 2004. Stabilité et contrôle des tourbillons d'une aile delta. Ph.D., Université Pierre et Marie Curie.

Rusak, Z., Wang, S., 1996. Review of theoretical approaches to the vortex breakdown phenomenon. AIAA Paper 96-2126.

Saffman, P.G., 1992. Vortex Dynamics. Cambridge University Press.

Sarkpaya, T., 1995. Vortex breakdown and turbulence. AIAA Paper 95-0433.

Sipp, D., Jacquin, L., 2000. Three-dimensional centrifugal-type instabilities of two-dimensional flows in rotating systems. Phys. Fluids 12 (7), 1740–1747.

Sipp, D., Fabre, D., Michelin, S., Jacquin, L., 2005. Stability of a vortex with a heavy core. J. Fluid Mech. 526, 67–76.

Tsai, S.E., Widnall, S.E., 1976. The instability of short waves on a straight vortex filament in a weak externally imposed strain field. J. Fluid Mech. 73, 721–733.

Tsai, C.Y., Widnall, S.E., 1980. Examination of group-velocity criterion for breakdown of vortex flow in a divergent duct. Phys. Fluids 23 (5), 864–870.

Vollmers, H., 2001. Detection of vortices and quantitative evaluation of their main parameters from experimental velocity data. Meas. Sci. Technol. 12, 1–9.

Werlé, H., 1982. Flow visualisation techniques for the study of high incidence aerodynamics. AGARD-VKI Lecture Series 121.

Zeman, O., 1995. The persistence of trailing vortices: a modeling study. Phys. Fluids 7, 135–143.